Interference Mitigation in Multibeam Satellite Networks as an Optimal Sublattice Problem

Francesco Lisi, *Graduate Student Member, IEEE*, Piero Angeletti, *Senior Member, IEEE*, João F. C. Mota, *Member, IEEE*, Julien Maurin, Hervé Legay, and George Goussetis, *Senior Member, IEEE*

Abstract-Resource distribution in radio networks aims at maximizing spectrum utilization while minimizing interference. In this paper, we consider the problem of uniform radio resource distribution on a periodic grid. We formulate the problem as finding the sublattice configuration that maximises the distance between adjacent resources, crucial for reducing interference and improving throughput performance. Leveraging concepts from lattice theory and discrete geometry, we present an enumerative, parallelizable algorithm to explore all possible sublattices and efficiently identify the optimal configurations. Additionally, we investigate the existence and properties of scaled-rotated sublattices, exploring how different lattice geometries impact optimal solutions. Numerical results demonstrate the effectiveness of the proposed algorithm and highlight insights into optimal sublattice design for various lattice structures. Furthermore, the results are applied to the identification of the beam layout in a fixed multibeam geostationary satellite. Numerical results show that the spectral efficiency of the optimised sublattice is higher than all other sublattices. This work thus advances the field of radio resource distribution and offers practical implications for improving satellite network performance.

Index Terms—Radio resource assignment, frequency reuse, wireless communications, satellite communications, lattice theory.

I. Introduction

In wireless networks, it is common practice to reuse the same frequency spectrum in different areas (cells), provided that such areas are sufficiently far apart to avoid interference. This technique, named frequency reuse, is widely used in broadcasting, mobile telephony, satellite communications and other radio services. It applies not only to frequency, but to any radio resource, e.g., polarization, spread spectrum code, or time slots. We refer to any of these resources as a *colour*. This technique was initially applied for planning broadcasting transmitters networks for AM or FM radio and television [1], but it found broader application in mobile-telephone services with the cellular concept [2]: instead of using one

F. Lisi is with the Antennas RF Systems R&T Department, Thales Alenia Space, 31037 Toulouse, France and also with the Institute of Signals, Sensors and Systems, Heriot-Watt University, EH14 4AS Edinburgh, Scotland, UK (e-mail: F.Lisi@hw.ac.uk). P. Angeletti is with the Secure Connectivity Space Segment Office, European Space Agency, ESA/ESTEC, 2200 AG Noordwijk, The Netherlands (e-mail: piero.angeletti@esa.int). J. F. C. Mota and G. Goussetis are with the Institute of Signals, Sensors and Systems, Heriot-Watt University, EH14 4AS Edinburgh, Scotland, UK (e-mail: j.mota@hw.ac.uk; g.goussetis@hw.ac.uk). J. Maurin is with the Antennas Service of the Architecture Department, Thales Alenia Space, 31037 Toulouse, France (e-mail: julien.maurin@thalesaleniaspace.com). H. Legay is with the Antennas RF Systems R&T Department, Thales Alenia Space, 31037 Toulouse, France (e-mail: herve.legay@thalesaleniaspace.com).

This work has been supported by the European Space Agency under contract No. 4000138743/22/NL/GLC/ov.

powerful transmitter to cover a large area, multiple lowerpower transmitters are strategically placed to create cells, each covering a smaller subarea. This led to a significant increase in overall network capacity.

Multibeam coverage in satellite communications. Frequency reuse is exploited in satellite communications systems to increase the total capacity by utilizing the same frequency band across multiple separate beams [3]. The transition from broadcast to broadband satellite services has intensified frequency reuse [4]. Broadband missions launched across low Earth orbit (LEO), medium Earth orbit (MEO), and geostationary Earth orbit (GEO) heavily rely on contiguous multibeam coverage, where large areas are served by a lattice of beams [4]. Narrower beams enhance gain, allowing the link budget requirements to be met with less stringent user antenna performance. Meanwhile, spectral resources can be reused across the lattice, thereby allowing higher throughput within given frequency allocations. Multibeam coverage is also central to emerging direct-to-device missions and standards [5].

Fixed multibeam coverage. Multibeam coverage is commonly implemented with the generation of a fixed lattice of uniform switchable beams. This is often the preferred approach even for satellites with digitally transparent payloads [6] and active antenna architectures, since real-time precoding and beamforming are incompatible with foreseeable processing capabilities [7]. The fixed lattice is split into periodic sublattices such that the beams of any given sublattice are sufficiently separated to avoid strong interference. The beams associated with a given sublattice are then served by the same frequency resource (colour). A notable example often adopted in GEO satellite communication networks is the 4-colour reuse scheme, where a hexagonal beam layout is split into 4 hexagonal sublattices, one for each colour [8]. Other popular choices for segmenting hexagonal lattices into sublattices of the same frequency and/or colour involve reuse factors of 3 or 7 [9]. A higher frequency reuse factor typically leads to lower interference at the cost of a reduced frequency resource serving each beam. In general, the objective is to select sublattices such that this trade-off is optimised.

Beam layout assignment per colour. In satellite communication networks the number of colours (i.e. reuse factor) is determined by a mix of system and regulatory constraints, including assigned number of frequency slots, polarization reuse, channelization aspects, antenna dispersion, and user terminal bandwidth. Given a periodic lattice of beams and a fixed number of colours, it remains an open problem to find an assignment between the colours and the beams such that the signal-to-interference-plus-noise ratio (SINR) is maximised.

2

Relation to TIM. Topological interference management (TIM) shows that, when only the binary interference topology is known, carefully designed time/frequency schedules can outperform hard frequency reuse [10]. However, the TIM gains shrink as the radius of strong interference grows: when each receiver is affected by many tiers of neighbours, the improvement on the number of degrees of freedom over static reuse becomes marginal [11]. This is precisely the operating regime of GEO broadband missions, where spot beams generate nonnegligible interference over tens of cells, as in the example in Sect.VI. Here, we address a different problem: for a given number of orthogonal resources C, we constructively find the sublattice that maximises the minimum co-channel distance between beams. User-beam association and fast scheduling are left to the radio resource management (RRM) layer and are outside the scope of this work.

Optimal solutions for canonical number of colours. The theory of lattices [12] and the theory of numbers [13] offer useful instruments to tackle this problem. The optimal solution depends on the underlying lattice and on the number of colours. Low order patterns for the hexagonal lattice were identified by Espley [14]. After introducing the mathematical basis of the geometry of lattices, Fastert [15] described a method of linear distribution of colours providing optimal minimum distances. Although limited to the particular case of progressive distribution of colours on parallel lines, [15] can be considered as the first application of the theory of lattices to the resource assignment problem. The arrangement of 2 frequencies and 2 polarizations (i.e. 4 colours) on a hexagonal lattice has been widely adopted in satellite networks [3]. It can be proven that an hexagonal placement of same colour cells over an hexagonal lattice maximises the distance between the closest neighbours assigned to the same colour. A solution to this instance for a generic number of colours was elaborated by Donald [2], who rediscovered a Diophantine quadratic equation on the permissible number of colours that had already been reported by Espley and attributed to E. V. Newbery and J. W. Ryde [14]. Algorithms generating optimal colour distributions on hexagonal lattices for arbitrary number of colours were presented in [16]. The use of quadratic Diophantine equations was extended by de Almeida and Palazzo [17] to square lattices, but erroneously considered optimal. Their approach replicates results of [18], which are also nonoptimal for square lattices.

Problem statement. The Diophantine equations in [2] and in [17] for hexagonal and square lattices, respectively, enable finding sublattices that are rotated and scaled versions of the original ones. These equations, however, have integer solutions only for a subset of colours *C*. Furthermore, while these solutions achieve the maximum spacing between nearest same-colour neighbours for hexagonal lattices, they do not for square ones. Therefore, there is no general procedure that, given an arbitrary number of colours and a lattice in arbitrary dimension, computes the optimal sublattice maximizing the distance between the closest neighbours assigned to the same colour. Finally, the similarity of the two Diophantine equations for the hexagonal and square lattices suggests the existence of a generalised equation applicable to a broader class of bi-

dimensional lattices. We thus aim to answer the following questions:

- 1) Given a regular lattice and an arbitrary number of colours, what is the partition into regular sublattices that maximises the distance between same-colour closest neighbours?
- 2) Given a regular lattice and an arbitrary number of colours, is it possible to find a sublattice that corresponds to a scaled-rotated version of the starting one?

The solution to 1) minimises the interference experienced by each user. The solution to 2) applies to direct radiating antenna (DRA) payloads with regularly spaced elements. In fact, these architectures enable exploiting the regularity of the nulls in the radiation patterns to mitigate interference [19], [20]. For example, if we consider a DRA with elements placed on a square lattice, the resulting radiation patterns will have nulls that are located on a square lattice. Consequently, if we start from a square beam layout, we would like to find a sublattice that is also square (eventually rotated). In that case, for all the colours, every beam centre is located on the nulls of the remaining beams assigned to the same colour.

Contributions. We summarize our contributions as:

- 1) We describe the maximum same-colour nearest neighbour distance sublattice (MASCONDS) algorithm. This is a non-redundant enumerative algorithm which, after applying a lattice reduction algorithm, explores all the possible sublattice representative bases and selects the one maximising the distance between the nearest neighbours with the same colour. The method generalizes well established results [14]-[18], [21], which can be obtained as particular cases of the unified approach. The bruteforce approach guarantees that the solution corresponds to a global optimum and outperforms discrete global optimization methods by avoiding the exploration of different solutions that correspond to the same sublattice. Although the results are detailed for the case bidimensional, the method can be applied "as is" to higherdimensional problems. The proposed method allows the identification of iso-colour cells by means of vectorialmodulo operation, as described in [22].
- 2) We generalize the Diophantine equations in [2], [16], [17] for the existence of scaled-rotated sublattices to a broader class of 2D lattices that includes the previous ones as special cases.
- 3) We apply the MASCONDS algorithm to design a fixed multibeam layout of a GEO communication satellite with a non-canonical number of colours. The solution provided by the algorithm results in higher spectral efficiency (SE) performance compared to all remaining sublattice configurations with the same number of colours.

Organization. The paper is organized as follows. In Sect. II, we cover the fundamentals of lattice theory and formulate the colour assignment problem. Sect. III presents our MASCONDS algorithm. Sect. IV then generalises the Diophantine equations to a broader class of 2D lattices. Numerical results for different underlying lattices are discussed in Sect. V. In Sect. VI, we apply the MASCONDS algorithm to compute

3

the optimal fixed multibeam layout for a GEO communication satellite. Conclusions follow in Sect. VII.

II. LATTICE THEORY AND PROBLEM FORMULATION

Lattice theory is a fundamental branch of mathematics dealing with the study of regular pattern of points in multidimensional spaces. Periodic lattices find applications across various scientific disciplines, including crystallography [23], materials science [24], cryptography [25], array processing [26] and satellite communications [7], where understanding and exploiting their underlying periodicity is fundamental.

Lattice. A uniform lattice over \mathbb{R}^N is an infinite discrete set of points defined as [26]

$$\Lambda(\mathbf{D}) = \left\{ \mathbf{r} \in \mathbb{R}^N : \mathbf{r} = \mathbf{D}\mathbf{n} = \sum_{i=1}^N n_i \mathbf{d}_i, \forall \mathbf{n} \in \mathbb{Z}^N \right\}, \quad (1)$$

where $D = [d_1, \ldots, d_N] \in \mathbb{R}^{N \times N}$ is a non-singular matrix. The *i*-th element of vector n, denoted by n_i , represents the number of steps along d_i . When N = 2, each lattice point can be expressed as $r = n_1 d_1 + n_2 d_2$. The most common 2D lattices are the square and hexagonal ones, whose D matrices correspond to

$$D_{\Box} = \begin{bmatrix} 1 & 0 \\ 0 & 1 \end{bmatrix}, \qquad D_{\bigcirc} = \sqrt{\frac{2}{\sqrt{3}}} \begin{bmatrix} \frac{\sqrt{3}}{2} & \frac{\sqrt{3}}{2} \\ -\frac{1}{2} & \frac{1}{2} \end{bmatrix}, \qquad (2)$$

where $\sqrt{2/\sqrt{3}}$ in D_{\bigcirc} guarantees $|\det D| = 1$. Given a lattice $\Lambda(D)$, any *unimodular* integer matrix $M \in \mathbb{Z}^{N \times N}$ (i.e. an integer matrix with unitary determinant, $|\det M| = 1$) produces a new base matrix D',

$$D' = DM, (3)$$

which generates the same lattice, i.e. $\Lambda(D) \equiv \Lambda(D')$. Consequently, any lattice can be associated to several different bases. Two matrices D and D', satisfying (3) for some integer unimodular M matrix are called *right-equivalent*.

Volume of a lattice. The volume of a lattice is defined as the volume of its cell, $vol(\Lambda) = |det D|$ (area in the 2D case), and is invariant to the choice of the basis, since |det M| = 1. The unit cell can be either the fundamental parallelogram or the Voronoi region [26].

Reduced-form D **matrix.** In the following, we assume that D is in reduced form, i.e. it always satisfies the two following properties:

$$||d_1|| \le ||d_2|| \le \dots \le ||d_N||,$$
 (4a)

$$\{d_i\}_{i=1}^N$$
 corresponds to the shortest vector lattice basis. (4b)

Sublattice. Given $\Lambda(D)$, a sublattice with C colours is a partition of the lattice into C interleaved lattices. Each sublattice can be obtained by translating the sublattice centred at the origin. An example of a sublattice with two colours is shown in Fig.1a, where the blue circles correspond to the sublattice centred at the origin and the red squares are obtained by applying a [1,0] translation. Mathematically, a sublattice of $\Lambda(D)$ corresponds to the lattice $\Lambda(DM)$, where $M \in \mathbb{Z}^{N \times N}$

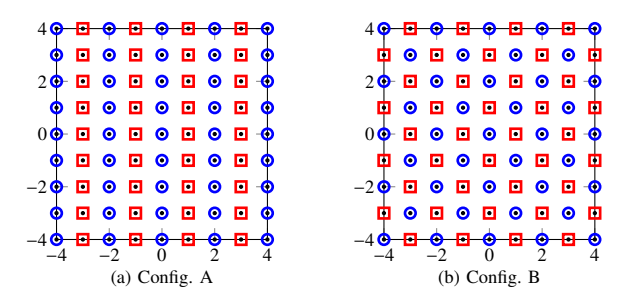


Figure 1: Plot of two different sublattices of a square lattice with 2 colours. Configuration B is also known as quincunx.

is an integer matrix with $|\det M| = C$. If we define $V \triangleq DM$, the following sublattice matrices

$$V_{\mathbf{A}} = \mathbf{D}_{\square} \mathbf{M}_{\mathbf{A}} = \begin{bmatrix} 1 & 0 \\ 0 & 1 \end{bmatrix} \begin{bmatrix} 0 & 2 \\ 1 & 0 \end{bmatrix} = \begin{bmatrix} 0 & 2 \\ 1 & 0 \end{bmatrix},$$

$$V_{\mathbf{B}} = \mathbf{D}_{\square} \mathbf{M}_{\mathbf{B}} = \begin{bmatrix} 1 & 0 \\ 0 & 1 \end{bmatrix} \begin{bmatrix} 1 & 1 \\ -1 & 1 \end{bmatrix} = \begin{bmatrix} 1 & 1 \\ -1 & 1 \end{bmatrix},$$
(5)

correspond to the ones in Fig.1a and Fig.1b, respectively.

Distance maximization problem. For a given number of colours C, a lattice can be partitioned into several possible sublattices. An important problem in communications (or resource allocation) is then finding the sublattice whose distances between the closest same-coloured neighbours is maximal. For example, in the two configurations in Fig.1, B is preferred over A, since the distance between the closest same-coloured neighbours is $\sqrt{2}$, whereas in A it is 1. Mathematically, the problem can be formulated as follows

$$M_{C}^{\star} \in \underset{\substack{M \in \mathbb{Z}^{N \times N} \\ \text{ldet } M \models C}}{\operatorname{max}} \min_{n \in \mathbb{Z}^{N} \setminus \{0\}} \|DMn\|,$$
(6)

where the \in operator is used instead of the equal sign, since there can be different optimal sublattices. Consider an example in \mathbb{R}^2 with C = 4, $D = D_{\square}$, and the following matrices

$$\mathbf{M}_1 = \begin{bmatrix} 2 & 0 \\ 0 & 2 \end{bmatrix}, \qquad \mathbf{M}_2 = \begin{bmatrix} 2 & 1 \\ 0 & 2 \end{bmatrix}. \tag{7}$$

Both matrices are optimal, as they achieve the maximum same-colour nearest-neighbour distance, i.e. $d_{\min} = 2$. However, while in the first case there are 4 neighbours with distance equal to 2, in the second one there are 2 neighbours within distance 2 and 2 neighbours within distance $\sqrt{5}$.

Next, we present an algorithm for solving (6).

III. MASCONDS ALGORITHM

The first step in solving (6) consists in enumerating all the possible sublattices of $\Lambda(D)$ that have C colours. Considering configuration A in Fig.1a, it can be observed that multiple M matrices generate the same sublattice. One possible choice corresponds to the matrix M_A in (5), while an alternative is

$$\mathbf{M}_{A}' = \begin{bmatrix} 0 & 2 \\ 1 & 1 \end{bmatrix},\tag{8}$$

which generates the same sublattice. In general, any discrete right-equivalent matrix of M_A results in the same sublattice regardless of the original lattice. Consequently, all the discrete

4

right-equivalent matrices of M_A generate the sublattice in Fig.1a. Analogously, all the right-equivalent matrices of M_B in (5) generate the sublattice in Fig.1b.

Hermite normal-form matrix. Given the above degree of freedom, we restrict our search to matrices that have a simple representation, namely Hermite normal-form matrices. A non-singular non-negative integer matrix \boldsymbol{H} is in Hermite normal-form if it satisfies the two following properties:

Integer upper triangular matrix:

$$H_{ij} = 0, \quad \forall i, j : 1 \le j < i \le N.$$
 (9a)

Off-diagonal elements smaller than pivot:

$$0 \le H_{ij} < H_{ii}, \forall i, j : 1 \le i < j \le N.$$
 (9b)

From property (9a) and (9b), it follows that

$$|\det \boldsymbol{H}| = \prod_{i=1}^{N} H_{ii} = C. \tag{10}$$

From the Hermite normal-form theorem, each sublattice is represented uniquely by only one Hermite normal-form matrix [27]. If we denote by $\mathcal{H}_{N,C} \in \mathbb{Z}^{N \times N}$ the set of Hermite normal-form matrices of size $N \times N$ with determinant equal to C, problem (6) can be reformulated as

$$M_C^{\star} \triangleq H_C^{\star} \in \arg \max_{H \in \mathcal{H}_{NC}} \min_{n \in \mathbb{Z}^N \setminus \{0\}} \|DHn\|.$$
 (11)

Hermite normal-form matrix generation. All the possible matrices in Hermite normal-form with determinant equal to C can be built as follows: first, we find all the combinations of positive integer diagonal entries that satisfy (10). For each pivot combination, the elements of each row are set to 0 if they are to the left of the pivot, as per (9a), and are set to non-negative integer values smaller than the pivot if they are to the right, as per (9b). As an example, for a 2D lattice (N = 2) with C = 4, all the possible sublattices are

$$\begin{bmatrix} 4 & 0 \\ 0 & 1 \end{bmatrix} \begin{bmatrix} 4 & 1 \\ 0 & 1 \end{bmatrix} \begin{bmatrix} 4 & 2 \\ 0 & 1 \end{bmatrix} \begin{bmatrix} 4 & 3 \\ 0 & 1 \end{bmatrix} \quad \begin{bmatrix} 2 & 0 \\ 0 & 2 \end{bmatrix} \begin{bmatrix} 2 & 1 \\ 0 & 2 \end{bmatrix} \quad \begin{bmatrix} 1 & 0 \\ 0 & 4 \end{bmatrix}.$$
(12)

The matrices within each of the three groups have the same pivot combination, i.e. (4,1), (2,2), and (1,4), respectively. One can check that each matrix generates a different sublattice. If $C = \prod_{t=1}^{P} p_t^{m_t}$, where p_t is a prime factor and m_t its multiplicity, the total number of pivot combinations is

$$\prod_{t=1}^{P} \binom{N-1+m_t}{N-1},\tag{13}$$

which corresponds to the number of partitions of the set $\{p_t : m_t, t = 1, ..., P\}$ into N subsets, where $p_t : m_t$ denotes a set with element p_t repeated m_t times. Since the partition of each prime factor is independent of the others, (13) corresponds to the product of the partitions of each prime factor separately. The latter problem is a well-known problem in combinatorics (stars and bars problem), whose solution can be found in [28].

The total number of distinct Hermite normal-form matrices of size $N \times N$ with determinant C is equal to [29]

$$L \triangleq \left| \mathcal{H}_{N,C} \right| = \prod_{i=1}^{P} \prod_{n=1}^{N-1} \frac{p_t^{m_t + n} - 1}{p_t^n - 1}.$$
 (14)

Algorithm 1 MASCONDS

Outputs:

 \boldsymbol{H}^{\star} , Optimal sublattice matrix $\boldsymbol{h}_{ij}^{\star} \in \mathbb{Z}, i, j = 1, \dots, N$

 $N \leftarrow \text{Size}(\boldsymbol{D}, 1)$

 $H_{\text{fil}} \leftarrow \text{GenerateHermiteNormalFormMatrices}(N,C)$

▶ $H_{(S)}$ is a cube of dimension (N, N, L) containing all the Hermite normal-form matrices as layers

$$\begin{array}{ll} L \leftarrow \operatorname{Size}(H,3) \\ \text{for } l = 1, \ldots, L \text{ do} \\ H \leftarrow H_{\text{sp}}(:,:,l) \\ V \leftarrow DH \\ V_{\text{sp}}(:,:,l) \leftarrow \operatorname{LatticeReductionAlgorithm}(V) \end{array} \Rightarrow \text{This loop can be parallelized}$$

ightharpoonup The reduced V matrix with columns sorted in ascending order of length is stored in the l-th layer of the V_{\varnothing} cube

end for $l_{\max} \leftarrow \arg\max_{l=1,\dots,L} \| \boldsymbol{V}_{\boldsymbol{\omega}}(:,1,l) \| \boldsymbol{H}^{\star} \leftarrow \boldsymbol{H}_{\boldsymbol{\omega}}(:,:,l_{\max})$

Lattice reduction. The second step in solving (11) consists in finding among all the Hermite normal-form matrices the one associated to the sublattice with the largest minimum distance. Since the total number of sublattices is finite, a brute force approach, where the minimum distance for each sublattice is computed, allows finding the optimal solution. In general, the matrix V = DH is not in reduced form, i.e. does not satisfy (4a) and (4b), so we start by running a lattice reduction algorithm. Lattice reduction algorithms can be classified into two categories: exact algorithms, with running times at least exponential in the dimension N, and approximate algorithms, with polynomial running times. The problem of lattice reduction has been studied extensively, e.g. [27]. Here, as we focus on 2D lattices, we apply the Lagrange algorithm [30], which is exact in 2D. Due to the exponential complexity of the lattice reduction problem on N, the proposed algorithm may become infeasible for high-dimensional cases. However, most applications in electromagnetism and communications deal with 2D or 3D lattices, so the algorithm can be run in a negligible amount of time compared to the other operations. MASCONDS Algorithm. The pseudo-code of the algorithm

MASCONDS Algorithm. The pseudo-code of the algorithm is described in Alg. 1. GenerateHermiteNormalFormMatrices generates all the Hermite normal-form matrices with *C* colours as detailed in the previous paragraphs, while LatticeReductionAlgorithm is any exact lattice reduction algorithm.

Parallelization. For each candidate Hermite normal-form matrix H in H_{ϖ} , we (i) form V = DH, (ii) apply a lattice-reduction routine to V, and (iii) evaluate the objective (minimum same-colour nearest neighbour distance) for that candidate. These per-candidate computations are independent, no data are shared across candidates, so the overall procedure can be parallelised. For example, in Matlab [31], Parfor distributes the computation across different cores, while arrayfun parallelizes the computation on the GPU.

Theorem 1. Given a non singular matrix $D \in \mathbb{R}^{N \times N}$ and an integer C > 0, Alg. 1 outputs a solution to problem (11).

Proof. Given C > 0, the prime factorization theorem [32] guarantees the uniqueness of the factorization $C = \prod_{t=1}^{P} p_t^{m_t}$.

Thus, the procedure described in (12), which the function GenerateHermiteNormalFormMatrices implements, generates the full set $\mathcal{H}_{N,C}$. The result follows by noticing that Alg. 1 (exhaustively) selects the matrix $\mathbf{H} \in \mathcal{H}_{N,C}$ associated with the sublattice whose minimum distance between same-coloured neighbours is maximal.

Computational complexity analysis. The computational complexity of Alg. 1 is dominated by the most expensive function inside the loop, the lattice reduction algorithm, whose complexity using the exact algorithm from [33] is $\tilde{O}(2^{2N})$. Although here we provide the asymptotic complexity of the algorithm in terms of N and C, it is worth mentioning that in most communication problems N is either 2 or 3, and C is typically smaller than 100.

Theorem 2. Alg. 1 has computational complexity $\tilde{O}(C^{N-1}2^{2N})$ if the for loop is run sequentially and $\tilde{O}(2^{2N})$ if run in parallel.

Proof. In both cases, the dominant operation in Alg. 1 is the lattice reduction algorithm inside the loop. From [33], it has complexity $\tilde{O}(2^{2N})$. So, if the loop is run in parallel, the complexity of Algorithm 1 is $\tilde{O}(2^{2N})$. On the other hand, if the loop is run sequentially, we need to multiply the previous expression by L. In Appendix A, we prove that $L = O\left(\ln(\max_t p_t)C^{N-1}\right)$, where $\max_t p_t$ is the largest prime factor of C. Consequently, the total complexity corresponds to $\tilde{O}(C^{N-1}2^{2N})$, where the $\ln(\max_t p_t)$ is neglected in the \tilde{O} (soft-O) notation.

Upper bound on the nearest-neighbour distance. We conclude this section by providing an upper bound on the nearest-neighbour distance of an N-dimensional lattice. The Hermite's constant of dimension N is defined as [30]

$$\gamma_N \triangleq \sup_{\Lambda \in \mathbb{R}^N} \left(\frac{d_{\min}(\Lambda)}{\operatorname{vol}(\Lambda)^{1/N}} \right)^2, \tag{15}$$

where

$$d_{\min}(\Lambda) \triangleq \min_{\boldsymbol{r} \in \Lambda \setminus \{0\}} \|\boldsymbol{r}\|. \tag{16}$$

Hermite was the first one to provide an upper bound on his constant, which is an exponential one, while in [30] the following linear bound is provided

$$\gamma_N \le 1 + \frac{N}{4}.\tag{17}$$

From (15), the following upper bound on the maximum minimum distance of any lattice Λ can be derived

$$d_{\min}(\Lambda)^2 \le \gamma_N \text{vol}(\Lambda)^{2/N}$$
. (18)

If we consider a sublattice with C colours, (18) becomes

$$d_{\min}(\Lambda(\mathbf{D}M))^{2} \leq \gamma_{N} \operatorname{vol}(\Lambda(\mathbf{D}M))^{2/N} = \gamma_{N} C^{2/N} |\det \mathbf{D}|^{2/N}.$$
(19)

The exact value of the Hermite's constant for $1 \le N \le 8$ and N = 24 are provided in [30]. In particular, for bi-dimensional lattices, $\gamma_2 = 2/\sqrt{3}$, which is achieved by the hexagonal lattice, where $d_{\min}(\Lambda(D_{\bigcirc}))^2 = 2/\sqrt{3}$ and $\operatorname{vol}(\Lambda(D_{\bigcirc})) = |\det D_{\bigcirc}| = 1$. Consequently, among all the planar lattices with the same unit cell size, i.e. same area, the hexagonal one guarantees the largest distance between neighbours. This

explains the reason why base stations should be arranged on an hexagonal lattice in a cellular network [2].

IV. SCALED-ROTATED SUBLATTICES

While an algorithm to find the optimal sublattice with C colours was presented in Sect. III, in this section we address the following question: given a lattice Λ , is it possible to find a matrix M that generates a sublattice with C colours that corresponds to a scaled and rotated version of Λ ? Such a solution is desirable in applications that require that the sublattice preserves the shape of the original one. For example, we would like to find all the C values that allow to generate a square sublattice from a square lattice.

Scaled-rotated sublattice existence condition. Mathematically, we know that the sublattice matrix can be expressed as V = DM, where we assume that D is the reduced original lattice matrix. However, if the sublattice matrix V must be a scaled and, eventually, rotated version of the original one D, then V must be also expressed as

$$V = DM = \sqrt[N]{C}RD, \tag{20}$$

where $R \in \mathbb{R}^{N \times N}$ is a rotation matrix $(R^{-1} = R^T, \det R = 1)$. The factor $\sqrt[N]{C}$ is necessary to ensure that $|\det V| = C |\det D|$. Since D is non-singular, we can express M as

$$M = \sqrt[N]{C} D^{-1} R D \in \mathbb{Z}^{N \times N}. \tag{21}$$

Consequently, given a lattice with reduced matrix D, a magnified sublattice with C colours can be found if and only if there exists a rotation matrix R such that the right hand side of (21) yields an integer matrix. One notable example corresponds to the case $\sqrt[N]{C} \in \mathbb{N}$ and $R = I_N$, where (21) becomes $M = \sqrt[N]{C}I_N$ regardless of D. Contrary to the previous example, the C values that admit a scaled-rotated sublattice depend on the chosen original lattice $\Lambda(D)$.

A special class of 2D lattices: SRC-2D lattices. In the following, we present some results for the bi-dimensional case, i.e. N=2. Since D is in reduced form, we can assume without loss of generality that $d_2 = \alpha R_{\phi} d_1$, where

$$\mathbf{R}_{\phi} \triangleq \begin{bmatrix} \cos \phi & -\sin \phi \\ \sin \phi & \cos \phi \end{bmatrix},\tag{22}$$

is a 2D rotation matrix and $\alpha \in [1, +\infty)$. Let us restrict our attention to the 2D lattices that are closed under the composite scaling-rotation operation, i.e. that satisfy the following property: $\forall v_1 \in \Lambda(D)$, then $v_2 = \alpha R_\phi v_1 \in \Lambda(D)$. To simplify the notation, we refer to this class of lattices as SRC-2D lattices. Rotationally symmetric lattices, such as the square and hexagonal ones, are special cases, where $\alpha = 1$, and $\phi = \pi/2$ and $\phi = \pi/3$, respectively. Since $v_1, v_2 \in \Lambda(D)$, then $v_1 = Dm_1$ and $v_2 = Dm_2$ with $m_1, m_2 \in \mathbb{Z}^2$. Consequently, the expression

$$Dm_2 = \alpha R_{\phi} Dm_1 \iff m_2 = \alpha D^{-1} R_{\phi} Dm_1 \qquad (23)$$

should provide an integer vector, i.e. $m_2 \in \mathbb{Z}^2$, for any $m_1 \in \mathbb{Z}^2$. The latter condition is met if and only if the matrix

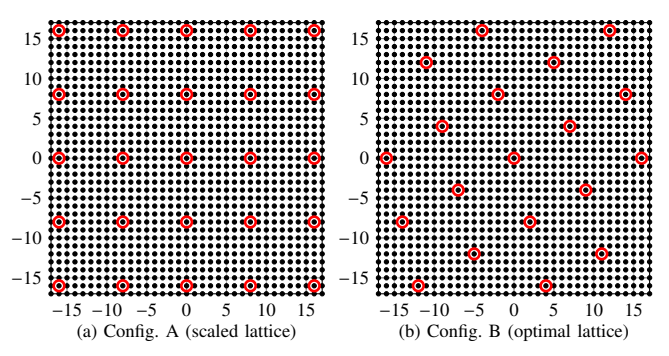


Figure 2: Plot of the scaled (a) and optimal (b) sublattice of a square lattice with 64 colours.

 $\alpha D^{-1} R_{\phi} D$ is an integer matrix. For the bi-dimensional case, the latter corresponds to

$$\alpha \mathbf{D}^{-1} \mathbf{R}_{\phi} \mathbf{D} = \begin{bmatrix} 0 & -\alpha^2 \\ 1 & 2\alpha \cos \phi \end{bmatrix}, \tag{24}$$

that is an integer matrix if and only if

$$\alpha = \sqrt{h_1}, \qquad h_1 \in \mathbb{N} \setminus \{0\},$$

$$\phi = \pm \arccos\left(\frac{h_2}{2\sqrt{h_1}}\right), \quad h_2 \in \mathbb{Z} : \left|\frac{h_2}{2\sqrt{h_1}}\right| < 1.$$
(25)

The pairs $(h_1 = 1, h_2 = 0)$ and $(h_1 = 1, h_2 = 1)$ both satisfy the conditions in (25) and correspond to the square and hexagonal lattice, respectively. However, the condition is also met by lattices whose reduced base vectors have different lengths, such as $(h_1 = 2, h_2 = 0)$, which is a rectangular lattice.

Scaled-rotated sublattice existence condition for SRC-2D lattices. By taking advantage of the special property of SRC-2D lattices, the condition in (21) is equivalent to the following one

$$\exists m_1 \in \mathbb{Z}^2 : ||Dm_1||^2 = C ||d_1||^2, \tag{26}$$

which can be expressed as

$$\exists \boldsymbol{m}_1 \in \mathbb{Z}^2 : \frac{\boldsymbol{m}_1^T \boldsymbol{D}^T \boldsymbol{D} \boldsymbol{m}_1}{\boldsymbol{d}_1^T \boldsymbol{d}_1} = C, \tag{27}$$

which corresponds to the general expression of the Diophantine equation [2], [16], [17]. Assuming that $m_1 = [i, j]^T$, for the square lattice, i.e. $D = D_{\square}$, (27) becomes

$$i^2 + j^2 = C, (28)$$

and for the hexagonal lattice, i.e. $D = D_{\cap}$

$$i^2 + ij + j^2 = C. (29)$$

These two cases have been extensively studied already, and the list of the first hundred integers that satisfy either (28) or (29) can be found in [16], [17].

Are scaled-rotated sublattices optimal? A question that then arises is whether, for those lattices that admit a scaled-rotated sublattice with C colours, the latter corresponds to the optimal sublattice, i.e. the one that maximises the same-colour nearest-neighbour distance. In general, the answer is negative. For example, Fig.2 shows two different configurations for a square lattice with 64 colours. Since $m_1 = [8,0]^T$ is a solution of (28), this lattice and number of colours combination admits

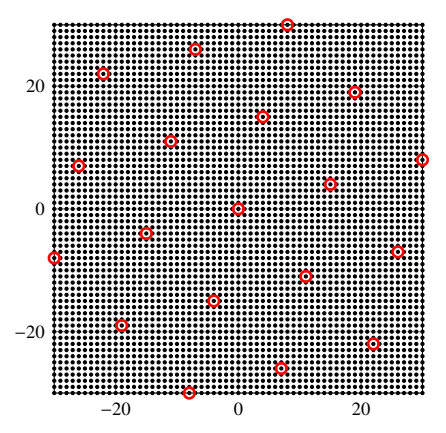


Figure 3: Optimal sublattice of a square lattice with C = 209. The resulting sublattice is close to a rotated hexagonal lattice.

a scaled-rotated sublattice, as shown in Fig.2a. However, the optimal sublattice, obtained with Alg. 1, does not correspond to the scaled one and is shown in Fig.2b. The \boldsymbol{M} matrices associated to the two configurations are

$$\mathbf{M}_{A} = \begin{bmatrix} 8 & 0 \\ 0 & 8 \end{bmatrix}, \qquad \mathbf{M}_{B} = \begin{bmatrix} 7 & -2 \\ 4 & 8 \end{bmatrix}, \tag{30}$$

that both have determinant equal to 64. Since $D_{\square} = I_2$, the minimum distance of the two configurations corresponds to 8 and $\sqrt{65} > 8$ for configuration A and B, respectively.

Optimality of the hexagonal sublattice. On the other hand, if the original lattice is hexagonal and admits a scaled-rotated sublattice for a given C, i.e. an integer solution of (29) exists, this also corresponds to the optimal one. The explanation is simple: the optimal bi-dimensional lattice is the hexagonal one, as anticipated in the last paragraph of Sect. III. To further emphasize this finding, we consider a sublattice of a square lattice that almost achieves the upper bound in (18), where $\operatorname{vol}(\Lambda) = \operatorname{vol}(\Lambda(D_{\square}M_{209}^*)) = |\det M_{209}^*| = 209$. Fig.3 shows the optimal sublattice obtained with the proposed algorithm. The corresponding M matrix is

$$\boldsymbol{M}_{209}^{\star} = \begin{bmatrix} 15 & 4\\ 4 & 15 \end{bmatrix}, \tag{31}$$

with $d_{\rm min}^2 = 241 < (2/\sqrt{3})209 \approx 241.33$. The two reduced sublattice base vectors have equal length and their angle corresponds to 60.14°, which is close to the 60° angle of an hexagonal lattice.

V. CLOSEST NEIGHBOUR DISTANCE ANALYSIS

Fig.4 represents the norm squared of the shortest and second shortest vectors in the sublattice as a function of the number of colours C. The starting lattice is the square lattice ($D = D_{\square}$) in Fig.4a, the hexagonal one ($D = D_{\bigcirc}$) in Fig.4b, and the isosceles triangular one in Fig.4c. The latter corresponds to the lattice $\Lambda(D_{\wedge})$ with

$$\boldsymbol{D}_{\Delta} \triangleq \begin{bmatrix} 1 & \frac{1}{2} \\ 0 & 1 \end{bmatrix}. \tag{32}$$

This is chosen as an example of a non conventional lattice, since $||d_1|| \neq ||d_2||$ contrary to the square and hexagonal cases.

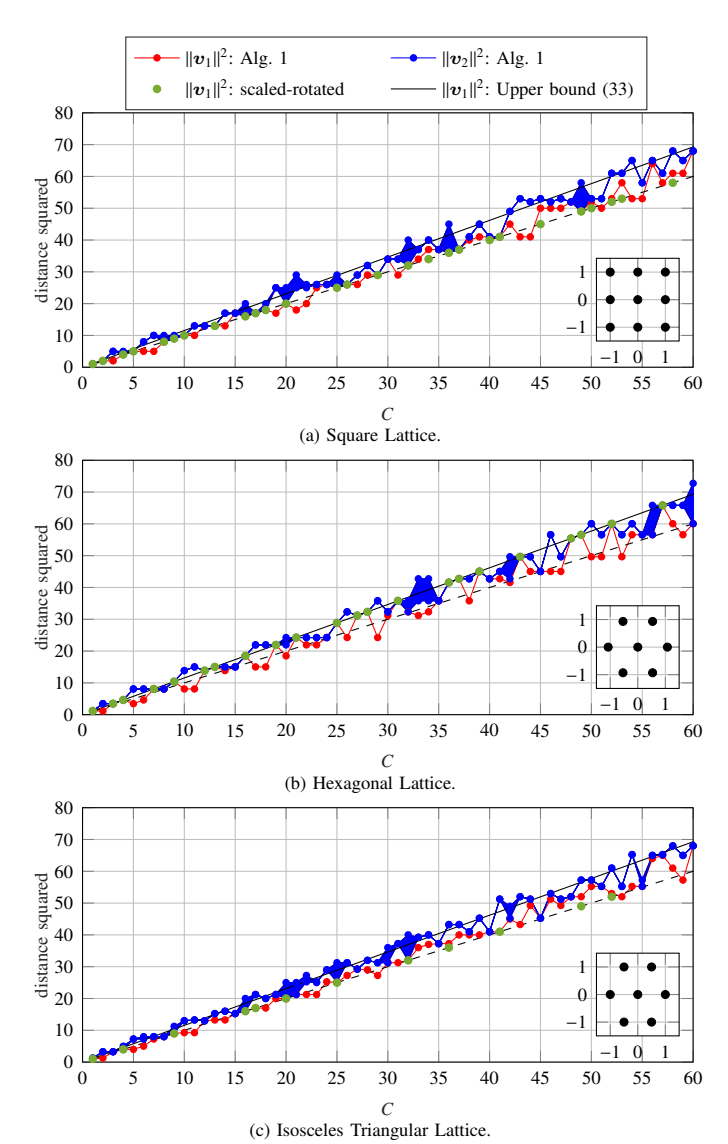


Figure 4: Plot of the squared norm of the first and second shortest sublattice vectors as a function of C. $V = [v_1, v_2]$ is the reduced sublattice matrix. The red and blue curves are obtained using Alg. 1. Since multiple lattices with different $||v_2||$ can achieve the same $||v_1||$, the blue region is the one subtended between the minimum and maximum values. The green dots correspond to scaled-rotated sublattices $(||v_2||^2 = ||v_1||^2)$ in (a) and (b), and $||v_2||^2 = (5/4) ||v_1||^2$ in (c)). The solid black line corresponds to the upper bound in (33).

Furthermore, since $\alpha = \sqrt{5}/2$ and $\phi = \arctan(2)$ do not satisfy the conditions in (25), this lattice does not belong to the class introduced in Sect. IV. Consequently, it is not sufficient to verify the Diophantine equation in (27) to assess that a scaled-rotated sublattice exists, (21) must hold instead.

Here we assume that $V = [v_1, v_2]$ is in reduced form, so v_1 and v_2 correspond to the first and second shortest vectors in the sublattice, respectively. Consequently, the red and green dots show how $d_{\min}^2 = ||v_1||^2$ changes with C for the optimal and scaled-rotated sublattices. Since the optimal solution is the one that maximises d_{\min} by definition, the red dots are always above or equal to the green ones.

The blue dots correspond to the norm squared of the second shortest vector, i.e. $||v_2||^2 \ge ||v_1||^2$, of the optimal sublattice obtained with the proposed algorithm. In general, more sub-

lattices can be optimal and achieve the maximum minimum distance, as anticipated in Sect. II. Therefore, different optimal solutions have the same $\|v_1\|$ value, but different $\|v_2\|$ values. This is captured in the figures by plotting the region subtended between the two extreme cases, i.e. the optimal solution with the smallest and largest $\|v_2\|$ value. For the scaled-rotated sublattices, the $\|v_2\|$ values are omitted. In fact, since the sublattice is a scaled-rotated version of the original lattice, the ratio between $\|v_2\|$ and $\|v_1\|$ corresponds to the one between $\|d_2\|$ and $\|d_1\|$. As a consequence, $\|v_2\|^2 = \|v_1\|^2$ for the square and hexagonal lattice, while $\|v_2\|^2 = (5/4)\|v_1\|^2$ for the isosceles triangular one.

By replacing vol (D) = 1 and $\gamma_2 = 2/\sqrt{3}$ in (19), we obtain the following upper bound on the minimum distance

$$||v_1||^2 = d_{\min}(\Lambda(V))^2 \le \frac{2}{\sqrt{3}}C.$$
 (33)

Finally, as a common feature of the three plots, we can observe that, depending on the starting lattice, not all C values support a scaled-rotated lattice, as introduced in Sect. IV. On the other hand, if C is a perfect square, a scaled lattice always exists regardless of the starting lattice, and $M = \sqrt{C}I_2$.

Considering the square lattice curves in Fig.4a, we can observe that the C values that support a scaled-rotated sublattice correspond to the ones that admit an integer solution of the Diophantine equation in (28). The reader can compare these values against the ones in [17]. From (20), it follows that $||v_1||^2 = C ||d_1||^2$ for the scaled-rotated sublattice, which explains the position of the green dots on the dashed line $||v_1||^2 = C$. In addition, the scaled-rotated solution does not correspond to the optimal one as discussed in Sect. IV and shown in Fig.2.

On the other hand, considering the curves in Fig.4b for the hexagonal lattice, the optimal solution corresponds to the scaled-rotated one when it exists. This is an expected result since the hexagonal lattice is the optimal planar lattice, i.e. the one that guarantees the largest spacing between same-colour neighbours given the unit cell area. Consequently, contrary to the square lattice case, here the upper bound is regularly achieved. Analogously to the square lattice case, the *C* values that support a scaled-rotated sublattice correspond to those that admit an integer solution of the Diophantine equation in (29), and they can be cross checked against the ones in [17].

Finally, Fig.4c shows the curves when the starting lattice corresponds to the isosceles triangular one. Since $||d_1|| = 1$ as in the square lattice case, the green dots are on the dashed line $||v_1||^2 = C$. Contrary to the two previous cases, since this lattice does not satisfy the conditions in (25), a rotation matrix R that satisfies (21) must be found for every C to prove the existence of a scaled-rotated sublattice. Like in the square lattice case, this sublattice does not correspond to the optimal one.

A general result that emerges from the three figures and is suggested by the upper bound expression is that d_{\min} grows as \sqrt{C} . Intuitively, if the area grows by a factor C, it is reasonable that the minimum distance grows as its square root. In general for N dimensional lattices, since the hyper-volume grows by C, the minimum distance grows by $\sqrt[N]{C}$ in line with the general expression of the upper bound in (18) with vol $(\Lambda) = C$.

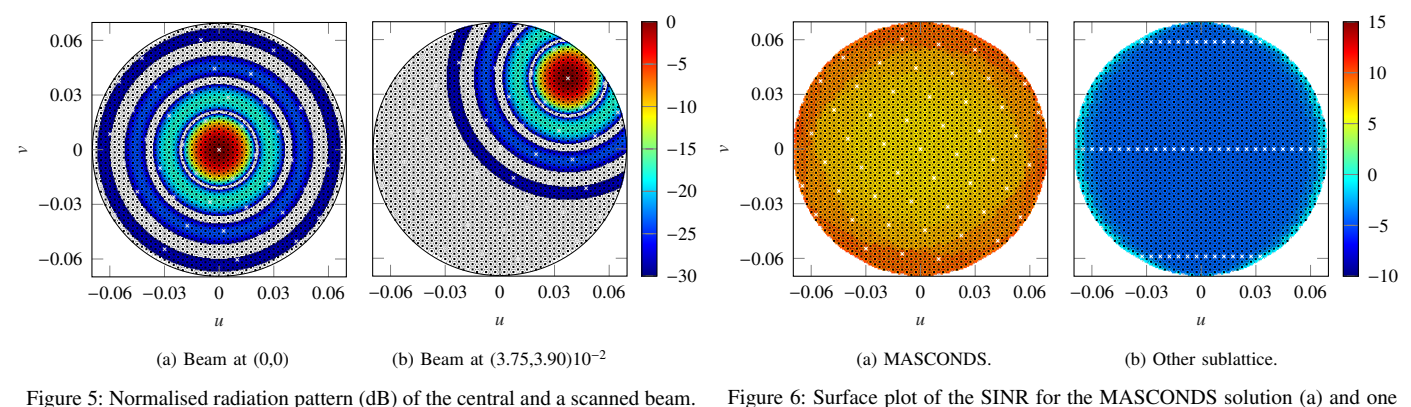


Figure 5: Normalised radiation pattern (dB) of the central and a scanned beam. The white crosses correspond to the beam centres for colour 1 considering the largest nearest-neighbour distance sublattice. The black crosses correspond to the beam centres of all the remaining colours.

applicable to any architecture. Fig.5a and Fig.5b illustrate the co-polar component pattern for the central beam and a scanned

of the remaining sublattices (b). The plot is obtained by considering all the

beams simultaneously active and by assigning the user to the closest beam.

The white crosses correspond to the beam centres for colour 1, while the

Finally, a note on the computational time required to compute the optimal sublattice using Alg. 1. Considering the case C = 999, it took an average of 2.5 ms to compute the optimal sublattice on a laptop with an intel[®] coreTMi5 processor with 1.3 GHz base speed, 10 physical cores, and a 16 GB RAM.

beam in the u-v plane. **Beam lattice and** C **selection.** Concerning the beam lattice, we consider a hexagonal beam lattice, since it allows to maximise the number of beams within the coverage, as described in Sect. III. The lattice spacing has been selected such that the distance between closest same-colour neighbours for the sublattice obtained with Alg. 1 corresponds to the -3dB beamwidth. Consequently, same-colour closest neighbours' beams overlap at -3dB. For C = 41, there are 42 different sublattices in total according to (14). However, due to the symmetry of the problem, these lead to only 8 different sets of results. As an example, by rotating 60° the sublattice in Fig.5a the results do not change.

VI. SATELLITE FIXED MULTIBEAM LAYOUT ASSIGNMENT

Link budget analysis. Assuming a line-of-sight propagation model as the one described in [7], the SINR experienced by user u in colour c is

In this section, we examine a Ku-band multi-beam GEO communication satellite use case where Alg. 1 is employed to compute a fixed grid of beams for a C value that does not support a scaled-rotated sublattice. Colours here represent any set of orthogonal resources, including CP-OFDM/OFDMA sub-carriers for 5G non-terrestrial network [34] or DFT-s-OFDM ones [35], [36]. The choice of C is constrained by regulatory or system requirements and cannot be arbitrary. As an example, we select C = 41, which proves to happen in practical implementations. The coverage considered is circular with a radius of 4° (sin(4°) in the *u-v* plane) consistent with typical scan ranges in GEO missions. While higher performance can be achieved by optimizing the antenna for a specific mission, such as European continental coverage, the industry trend is shifting towards reconfigurable, softwaredefined payload solutions that enable the same platform to be used for various missions. This shift justifies the adoption of a simple circular coverage.

$$SINR_{u}^{(c)} = \frac{S_{ub_{u}^{(c)}}^{(c)}}{1 + \sum_{lb' \neq b^{(c)}} S_{u,b'}^{(c)}},$$
(34)

Antenna model. To simplify the problem, we consider the right-hand circularly polarized electric field radiated by a circular aperture with a diameter of 1.5m and uniform amplitude illumination [37]. A linear phase shift is applied to steer the beam. The corresponding antenna gain is 45.3 dBi for the central beam and decays as $\cos \theta$ when scanning. A total radiated power of 7 kW is distributed over a bandwidth of 2 GHz, resulting in a power spectral density (PSD) of $\mathcal{P} = 3.5 \cdot 10^{-6}$ W/Hz. When the power is uniformly distributed across the beams, the PSD per beam corresponds to $\mathcal{P}/N_B^{(c)}$, where $N_R^{(c)}$ corresponds to the number of beams in colour c. While in a DRA architecture the beams are radiated by an active electronically scanned array, the uniform aperture model allows for an analytical computation of the radiated field and minimises the number of parameters requiring optimization. Despite its simplicity, this model provides meaningful results when all the beams are simultaneously active (worst case scenario). $b_u^{(c)}$ is the closest beam to user u in colour c, and

$$S_{ub}^{(c)} \triangleq \frac{\mathcal{P}}{N_{R}^{(c)}} \left(\frac{\lambda_{c}}{4\pi r_{u}}\right)^{2} \frac{G_{ub}^{(\mathrm{Tx})}}{k_{B}} \frac{G^{(\mathrm{Rx})}}{T^{(\mathrm{Rx})}},$$
 (35)

where $G_{ub}^{(\mathrm{Tx})}$ is the gain of beam b at the location of user u, r_u is the distance between the satellite and user u, λ_c is the free space wavelength of colour c, k_B is Boltzmann's constant, and $G^{(\mathrm{Rx})}/T^{(\mathrm{Rx})}$ is the receiver G/T, which is set to $10^{17/10}$ for all the users. In (34), we assumed that the colours are orthogonal, i.e. users assigned to different colours do not interfere, and same-colour interference is treated as additional noise (no interference cancellation). Fig.6 shows the SINR experienced by a user in every coverage position when it is assigned to the closest beam and all the other same-colour beams are active. Fig.6a corresponds to the MASCONDS algorithm's sublattice, and Fig.6b to one alternative sublattice.

Spectral efficiency evaluation. To evaluate the performance, we compare the SE considering all possible sublattices. The

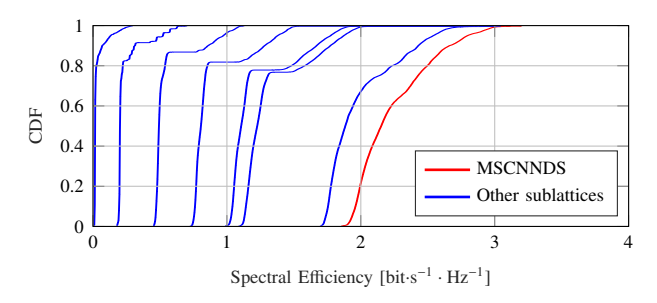


Figure 7: CDF of the DVB-S2X SE for all sublattices with C=41 of an hexagonal lattice. The red curve represents the MASCONDS solution, whose SINR is reported in Fig.6a. The blue curves represent all the remaining sublattices. Fig.6b corresponds to the second curve from the left.

SE is computed from the SINR as $\eta = \eta_{DVB-S2X}(SINR)$, where $\eta_{\rm DVB-S2X}(\cdot)$ is a third-order polynomial that interpolates the values in Table 20a in [38], which provides the SE obtained with adaptive coding and modulation for different E_s/N_0 values, where E_s is the energy per symbol and N_0 is the receiver noise spectral density. Fig.7 shows the cumulative distribution function (CDF) of the SE for the entire user population across all sublattices. The red curve represents the SE for the MASCONDS solution, while the blue curves represent the SE for all other sublattices. By comparing the curves, we can conclude that the MASCONDS solution provides the best SE distribution. This can be explained by looking at the SINR distribution in Fig.6. While all solutions have the same total number of beams distributed across the C = 41 colours, the MASCONDS one in Fig.6a guarantees the best SINR distribution because of the larger distance between same-colour neighbours, which results in lower interference. On the other hand, the solution in Fig.6b, which corresponds to the second curve from the left in Fig.7, experiences low SINR values due to the proximity of same-colour beams. Finally, if atmospheric losses were included in the analysis, all solutions would experience lower SINR, therefore, SE values. However, the MASCONDS solution would still provide the best SE over all sublattices.

Not an RRM algorithm. We conclude with an important observation. This section does not address the RRM problem in a multi-beam satellite. Instead, it introduces a sublatticebased methodology for determining the beam centres in a fixed multibeam communication satellite with C = 41 orthogonal resources. Once the precoding weights of the fixed beam are calculated and stored in memory, the DTP executes a lowcomplexity RRM algorithm, such as the H-RRM approach described in [39], to assign each user to a colour based on the current traffic distribution. In the resulting assignment, not all users are allocated to their closest beam. This is because, in some cases, two users may share the same closest beam while a neighbouring beam remains unassigned. In such scenarios, the RRM algorithm assigns one user to the closest beam and the other to the neighbouring beam with a different colour. As shown in Fig.5, each beam covers multiple cells of the hexagonal lattice. Nonetheless, the results presented in this section confirm that the MASCONDS is the ideal candidate for a uniform beam placement in a fixed multibeam payload.

VII. Conclusions

This paper addressed the critical issue of optimally distributing the available resources in a fixed multibeam satellite. By formulating the problem as a maximization of the distance between same-colour nearest neighbours within a periodic lattice, we have presented an enumerative algorithm that efficiently explores all possible sublattice configurations to identify the optimal solutions. Leveraging concepts from lattice theory, our approach offers a systematic method for attacking the problem.

Through extensive numerical results, we have demonstrated the effectiveness of our algorithm in identifying optimal sublattice configurations for various lattice structures. Our results highlight the importance of considering not only the spatial arrangement of resources but also the underlying lattice geometry in radio resource distribution. Additionally, we have investigated the existence and properties of scaled-rotated sublattices, providing insights into alternative configurations that may offer comparable performance to optimal solutions.

The implications of our findings extend beyond theoretical considerations, offering practical guidance for improving throughput performance. Although we focused on a GEO communication satellite use case, our approach can be applied as is to any other use case involving lattices and resource reuse, such as LiFi networks [40]. Moreover, our approach provides a foundation for future research in sublattice optimization, paving the way for non-exhaustive search strategies within a reduced space of all possible solutions.

$\begin{array}{c} \text{Appendix A} \\ \text{Limiting behaviour (order) of } L \end{array}$

Here, we derive the order of L in (14) as a function of N and C > 1. From (14), we can derive the following inequality

$$L \triangleq \prod_{t=1}^{P} \prod_{n=1}^{N-1} \frac{p_t^{n+m_t} - 1}{p_t^n - 1} \le \prod_{t=1}^{P} \prod_{n=1}^{N-1} \frac{p_t^{n+m_t}}{p_t^n - 1} = C^{N-1} \prod_{t=1}^{P} \prod_{n=1}^{N-1} \frac{p_t^n}{p_t^n - 1},$$
(36)

where we used $C = \prod_{t=1}^{P} p_t^{m_t}$ in the last step. Equality holds in (36) when the multiplicities of the prime factors tend to infinity. Taking the natural logarithm of the second term in (36), we obtain the following

$$\ln\left(\prod_{t=1}^{P}\prod_{n=1}^{N-1}\frac{p_{t}^{n}}{p_{t}^{n}-1}\right) = \sum_{t=1}^{P}\sum_{n=1}^{N-1}\ln\left(\frac{p_{t}^{n}}{p_{t}^{n}-1}\right) \\
\leq \sum_{p\in\mathcal{P}(\max_{t},p_{t})}\sum_{n=1}^{+\infty}\ln\left(\frac{p^{n}}{p^{n}-1}\right),$$
(37)

where $\mathcal{P}(m) = \{ p \in \mathbb{P} : 2 \le p \le m \}$ is the set of all the prime numbers smaller than or equal to m. We show below that

$$\lim_{m \to +\infty} \left[\sum_{p \in \mathcal{P}(m)} \sum_{n=1}^{+\infty} \ln \left(\frac{p^n}{p^n - 1} \right) - \ln \left(\ln \left(m \right) \right) \right] = K \approx 1.4079,$$
(38)

converges. The value of K has been obtained numerically. Therefore, when $\max_t p_t$ is large enough,

$$L \le C^{N-1} e^{\sum_{p \in \mathcal{P}(\max_t p_t)} \sum_{n=1}^{+\infty} \ln\left(\frac{p^n}{p^n-1}\right)} \sim C^{N-1} e^K \ln\left(\max_t p_t\right).$$
 (39)

We conclude that

$$L = O\left(\ln\left(\max_{t} p_{t}\right) C^{N-1}\right). \tag{40}$$

To show the convergence of (38), we start by expressing the sequence in (38) as the sum of two sequences as follows

$$f[m] \triangleq \sum_{p \in \mathcal{P}(m)} \sum_{n=1}^{+\infty} \ln\left(\frac{p^n}{p^n - 1}\right) - \ln\left(\ln\left(m\right)\right)$$

$$= \left(\sum_{p \in \mathcal{P}(m)} \ln\left(\frac{p}{p - 1}\right) - \ln\left(\ln\left(m\right)\right)\right) + \sum_{p \in \mathcal{P}(m)} \sum_{n=2}^{+\infty} \ln\left(\frac{p^n}{p^n - 1}\right)$$

$$= a[m] + b[m].$$

The sequence b[m] is bounded as follows

$$0 \leq b[m] \triangleq \sum_{p \in \mathcal{P}(m)} \sum_{n=2}^{+\infty} \ln\left(\frac{p^{n}}{p^{n}-1}\right) = \sum_{p \in \mathcal{P}(m)} \sum_{n=2}^{+\infty} \ln\left(1 + \frac{1}{p^{n}-1}\right)$$

$$\leq \sum_{p \in \mathcal{P}(m)} \sum_{n=2}^{+\infty} \frac{1}{p^{n}-1} = \sum_{p \in \mathcal{P}(m)} \frac{1}{p-1} \sum_{n=2}^{+\infty} \frac{1}{\sum_{n'=0}^{n-1} p^{n'}}$$

$$\leq \sum_{p \in \mathcal{P}(m)} \frac{1}{p-1} \sum_{n=2}^{+\infty} \frac{1}{p^{n-1}} = \sum_{p \in \mathcal{P}(m)} \frac{1}{(p-1)^{2}} \leq \frac{\pi^{2}}{6}.$$

$$(42)$$

where the first inequality follows from $\ln(1+x) \le x$, $\forall x \ge 0$, and the last one from the series $\sum_{k=1}^{+\infty} 1/k^2 = \pi^2/6$. Since b[m] is monotonically increasing and bounded, we can conclude that it converges. On the other hand, a[m] converges to [41]

$$\lim_{m \to +\infty} a[m] = \gamma,\tag{43}$$

where γ corresponds to the Euler-Mascheroni constant. Therefore, the sequence f[m] converges as the sum of two converging sequences.

REFERENCES

- [1] J.-F. Arnaud, "Frequency planning for broadcast services in Europe," *Proceedings of the IEEE*, Vol. 68, No. 12, pp. 1515-1522, Dec. 1980.
- [2] V. H. M. Donald, "Advanced mobile phone service: The cellular concept," *The Bell System Technical Journal*, Vol.58, No.1, pp.15-41, 1979.
- [3] J. C. Fuenzalida and E. Podraczky, "Reuse of the Frequency Spectrum at the Satellite," in Communication satellites for the 70's: systems - A collection of technical papers selected from the AIAA 3rd Communications Satellite Systems Conference, Apr. 1970.
- [4] R. De Gaudenzi, P. Angeletti, D. Petrolati, and E. Re, "Future technologies for very high throughput satellite systems," *International Journal of Satellite Communications and Networking*, vol. 38, no. 2, pp. 141–161, Mar. 2020.
- [5] Satellite Earth Stations and Systems (SES); Satellite Digital Radio (SDR) service; Functionalities, architecture and technologies, document ETSI TR 102 525 V1.1.1, Sep. 2006.
- [6] C. Nicolas, V. Enjolras, P. Voisin, C. Boustie, and G. Jestin, "Thales Alenia Space 6th Generation Digital Transparent Processor (DTP6G)-A Multi-mission, Multi-Mode Versatile Product at the Hearth of TELE-COM Solutions," *IET Conference Proceedings*, vol. 2022, no. 29, pp. 25–32, 2022.
- [7] P. Angeletti and R. De Gaudenzi, "A pragmatic approach to massive MIMO for broadband communication satellites," *IEEE Access*, Vol. 8, pp. 132212-132236, 2020.
- [8] R. Battaglia, R.Mizzoni, "Developments on Ka-band antennas for commercial geostationary communication satellites at Alenia Spazio", Proceedings of the 7th Ka Band Utilization Conference, 2001.
- [9] E. Björnson, E. G. Larsson, and M. Debbah, "Massive MIMO for maximal spectral efficiency: How many users and pilots should be allocated?," *IEEE Transactions on Wireless Communications*, vol. 15, no. 2, pp. 1293-1308, Feb. 2016.

- [10] S. A. Jafar, "Topological interference management through index coding," *IEEE Transactions on Information Theory*, vol. 60, no. 1, pp. 529–568, 2014.
- [11] Y. Gao, G. Wang, and S. A. Jafar, "Topological interference management for hexagonal cellular networks," *IEEE Transactions on Wireless Communications*, vol. 14, no. 5, pp. 2368–2376, May 2015.
- [12] T. W. S. Cassels, An introduction to the Geometry of Numbers, Springer-Verlag, Berlin Heidelberg, 1959.
- [13] H. Hasse, Number Theory, Springer-Verlag, Berlin Heidelberg, 1980.
- [14] D. C. Espley, "Optimum spacing of broadcast transmitters," Wireless Engineer, Vol. 28, No. 329, pp. 37-39, Feb. 1951.
- [15] H. W. Fastert, "Die mathematischen Grundlagen der theoretischen Sendernetzplanung," Ruridfunktechnische Mitteilungen, Vol. 4, pp. 48-56, 1960.
- [16] A. Gamst, "Homogeneous distribution of frequencies in a regular hexagonal cell system," *IEEE Transactions on Vehicular Technology*, Vol. 31, No. 3, pp. 132-144, Aug. 1982.
- [17] C. de Almeida and R. Palazzo, "On the frequency allocation for mobile radio telephone systems," *Proceedings of 6th International Symposium* on *Personal, Indoor and Mobile Radio Communications*, Toronto (ON), Canada, 1995.
- [18] J. Denes and A. D. Keedwell, "Frequency allocation for a mobile radio telephone system," *IEEE Transactions on Communications*, Vol. 36, No. 6, pp. 765-767, June 1988.
- [19] M. Pellet, G. Goussetis, H. Legay, J. Mota, P. Angeletti, and G. Toso, "Multibeam Phased Arrays Exploiting Frequency Dispersion for Massive MIMO Satellite Communications," in 18th European Conference on Antennas and Propagation, EuCAP 2024, 2024.
- [20] M. Pellet, G. Goussetis, J. Mota, H. Legay, and F. Vidal, "Multibeam Coverage Optimization for Broadband Satellites with Hybrid Beamforming Direct Radiating Arrays," in 2023 IEEE International Symposium on Antennas and Propagation and USNC-URSI Radio Science Meeting (USNC-URSI), pp. 1541–1542, Sep. 2023.
- [21] R. A. Leese, "A unified approach to the assignment of radio channels on a regular hexagonal grid," *IEEE Transactions on Vehicular Technology*, Vol. 46, No. 4, pp. 968-980, Nov. 1997.
 [22] P. Angeletti, "Simple implementation of vectorial-modulo operation
- [22] P. Angeletti, "Simple implementation of vectorial-modulo operation based on fundamental parallelepiped", *Electronics Letters*, Vol. 48, No. 3, pp. 159-160, Feb. 2012.
- [23] D. E. Sands, Introduction to Crystallography, Benjamin Cummings, 1978
- [24] W. D. Callister Jr., D. G. Rethwisch, Materials Science and Engineering: An Introduction, 10th Ed, Wiley, 2018.
- [25] D. Micciancio, O. Regev, "Lattice-based cryptography," in D.j. Bernstein, J. Buchmann, E. Dahmén (eds), *Post-quantum cryptography*, Springer, Berlin, 2008.
- [26] P. Angeletti, "Multiple Beams From Planar Arrays," *IEEE Transactions on Antennas and Propagation*, Vol. 62, No. 4, pp. 1750-1761, Apr. 2014.
- [27] G. Cortelazzo and R. Manduchi, "On the determination of all the sublattices of preassigned index and its application to multidimensional subsampling," *IEEE Transactions on Circuits and Systems for Video Technology*, Vol. 3, No. 4, pp. 318-320, Aug. 1993.
- [28] W. Feller, An Introduction to Probability Theory and Its Applications, Volume 1, 3rd ed. New York, NY, USA: John Wiley & Sons, p.38, 1968.
- [29] B. Gruber, "Alternative formulae for the number of sublattices," Acta Crystallographica Section A, vol. 53, no. 6, pp. 807–808, Nov. 1997.
- [30] P. Q. Nguyen, "Hermite's Constant and Lattice Algorithms," in P. Q. Nguyen, and B. Vallée (Eds), The LLL algorithm: survey and applications. Information security and cryptography, Springer, Berlin Heidelberg, pp. 19-69, 2010.
- [31] MATLAB. Accessed: Aug. 16, 2025. [Online]. Available: https://www.mathworks.com/products/matlab.html
- [32] G. H. Hardy and E. M. Wright, An Introduction to the Theory of Numbers, 6th ed. Oxford, U.K.: Oxford University Press, 2008, § 14.6.
- [33] D. Micciancio and P. Voulgaris, "A deterministic single exponential time algorithm for most lattice problems based on Voronoi cell computations," Proceedings of the Annual ACM Symposium on Theory of Computing, ACM, 2010, pp. 351–358.
- [34] 5G; NR; Physical channels and modulation (3GPP TS 38.211 version 18.6.0 Release 18), document ETSI TS 138 211 V18.6.0, Apr. 2025.
- [35] Satellite Earth Stations and Systems (SES); SC-FDMA based radio waveform technology for Ku/Ka band satellite service, document ETSI TR 103 297 V1.1.1, Jul. 2017.
- [36] H. Shahid et al., "Emerging Advancements in 6G NTN Radio Access Technologies: An Overview," 2024 Joint European Conference on Networks and Communications and 6G Summit, EuCNC/6G Summit 2024, pp. 593–598, 2024.

- [37] C. A. Balanis, Antenna Theory: Analysis and Design, 4th ed., John Wiley & Sons. 2015.
- [38] Digital Video Broadcasting (DVB); Second generation framing structure, channel coding and modulation systems for Broadcasting, Interactive Services, News Gathering and other broadband satellite applications; Part 2: DVB-S2 Extensions (DVB-S2X), document ETSI EN 302 307-2 V1.4.1, Aug. 2024.
- [39] P. Angeletti and R. De Gaudenzi, "Heuristic Radio Resource Management for Massive MIMO in Satellite Broadband Communication Networks," *IEEE Access*, vol. 9, pp. 147164–147190, 2021.
- [40] H. Haas, L. Yin, Y. Wang, and C. Chen, "What is LiFi?," J. Lightwave Technol., vol. 34, no. 6, pp. 1533-1544, Mar. 2016.
- [41] E. W. Weisstein, "Euler-Mascheroni Constant," MathWorld—A Wolfram Web Resource. [Online]. Available: https://mathworld.wolfram.com/Euler-MascheroniConstant.html. [Accessed: 21-Feb-2025].



Julien Maurin has been an antenna engineer at Thales Alenia Space since 2016, specializing in antenna modelling and simulation. He holds an engineering degree in electronics and microwaves from INP-ENSEEIHT (2012) and a Ph.D. in electromagnetics and high-frequency systems from the University of Toulouse (2015). His expertise includes the analysis and performance optimization of space antenna systems.



Francesco Lisi (S'22) received the B.Sc. (2019) and M.Sc. (2021) degrees in telecommunications engineering from the University of Florence and the University of Pisa, respectively. In 2021 he was a visiting student with the Laboratoire des Signaux et Systèmes, CentraleSupélec. From Nov. 2021 to Dec. 2022 he was with the Microwave and Radiation Laboratory, University of Pisa. Since 2023 he has been a Ph.D. student at Heriot–Watt University. In July 2024 he joined the Antenna R&T Department, Thales Alenia Space, Toulouse, developing payload

solutions for reconfigurable GEO satellites. From Nov. 2024 to Feb. 2025 he was a visiting researcher with ESA's Antenna and Sub-Millimetre Waves Section. He received the AEIT Renato Mariani Prize (2022) and was shortlisted for the EuCAP 2023 Best Student Paper Award. His interests include array processing, RRM algorithms, and array-fed reflectors.



Piero Angeletti (M'07–SM'13) received the Laurea degree in Electronics Engineering (summa cum laude) from the University of Ancona (IT) in 1996, and the Ph.D. in Electromagnetism from the University of Rome "La Sapienza" (IT) in 2010. Since 2004 he is with the European Space Research and Technology Center (ESTEC) of the European Space Agency (ESA), Noordwijk (NL). In his role as Head of the Secure Connectivity Space Segment Office he oversees the ESA design and development activities related to IRIS² (Infrastructure for Resilience,

Interconnectivity and Security by Satellite) space segment. Together with Dr G. Toso, he is instructor of the course on "Multibeam Antennas and Beamforming Networks", offered, since 2012, at main IEEE, EurAAP and EUMA conferences. They also organize the EurAAP-ESoA course on Active Antennas (2021, 2023, 2025). In 2022 he received the S. A. Schelkunoff award by the IEEE AP-S for the best IEEE TAP paper of 2021. In 2023 he has been appointed IEEE MTT-S and AP-S Inter-Society Distinguished Lecturer.



João F. C. Mota received the M.Sc. and Ph.D. degrees in electrical and computer engineering from the Technical University of Lisbon, Lisbon, Portugal, in 2008 and 2013, respectively, and the Ph.D. degree in electrical and computer engineering from Carnegie Mellon University, Pittsburgh, PA, USA, in 2013. He is currently an Assistant Professor of Signal and Image Processing with Heriot-Watt University, Edinburgh, U.K. His research interests include theoretical and practical aspects of high-dimensional data processing, inverse problems, op-

timization theory, machine learning, data science, and distributed information processing and control. Dr. Mota was a recipient of the 2015 IEEE Signal Processing Society Young Author Best Paper Award and is currently Associate Editor for IEEE Transactions on Signal Processing.



Hervé Legay received the Electrical Engineering and Ph.D. degrees from the National Institute of Applied Sciences, Rennes, France, in 1988 and 1991, respectively. Then, he was a Post-Doctoral Fellow with the University of Manitoba, Winnipeg, MB, Canada. In 1994, he joined Alcatel Space (now Thales Alenia Space), Toulouse, France. He initially conducted studies in areas of military telecommunication satellite antennas and antenna processing. He designed the architecture and the anti-jamming process of the first French space active antenna

(Syracuse 3 Program). He is currently the Head of Antenna, RF and System R&T Activities, coordinating Research activities on Advanced Antennas Concepts, innovative flexible payloads, and associated system engineering. He is Senior Expert on Antennas and the Chair of the Group of Antenna Experts at Thales Group. He is also managing the strategic academic partnerships for Thales Alenia Space, in charge of the implementation of an open innovation policy with academic and research partners. He has authored 50 patents. He conducted major developments on reflectarrays, full metal radio frequency (RF) metasurfaces, integrated and low-profile antennas, and multiple beam quasi-optical beamformers. His research interests include innovative active antenna architectures, MIMO processing, and system activities related to the monitoring of active antennas.



George Goussetis (S'99–M'02–SM'12) graduated Electrical and Computer Engineering at the National Technical University of Athens, Greece, in 1998, and obtained his Ph.D. from the University of Westminster, London, UK, in 2002. In 2002 he also graduated B.Sc. in physics (first class) from University College London (UCL), UK. In 1998, he joined Space Engineering (now Airbus DS) in Italy, as RF Engineer and in 1999 the University of Westminster, UK, as a Research Assistant. Between 2002 and 2006 he was a Senior Research Fellow at

Loughborough University, UK. He was Assistant Professor with Heriot-Watt University, Edinburgh, UK between 2006 and 2009 and Associate Professor with Queen's University Belfast, UK, between 2009 and 2013. In 2013 he joined Heriot-Watt and was promoted to Professor in 2014. He is currently the Associate Executive Dean for Enterprise at Heriot-Watt University. He has authored or co-authored over 500 peer-reviewed papers, several book chapters, one book, and six patents. His research interests are in the area of microwave and antenna components and subsystems with particular focus on their applications in satellite systems.

Dr. Goussetis held research fellowships from the Onassis foundation in 2001, the UK Royal Academy of Engineering between 2006-2011, and European Commission Marie-Curie in 2011-12 and again in 2014-17. He is the recipient of several awards including the 2011 European Space Agency young engineer of the year prize, the 2016 Bell Labs prize and the best IEEE Proceedings paper 2024. Dr. Goussetis served as Associate Editor to the IEEE Antennas and Wireless Propagation Letters between 2014-18 and as Chair of the European Conference of Antennas and Propagation (EuCAP) 2024.